Radiology

Glioblastoma: Vascular Habitats Detected at Preoperative Dynamic Susceptibility-weighted Contrast-enhanced Perfusion MR Imaging Predict Survival[1]

Javier Juan-Albarracín, MSc
Elies Fuster-Garcia, PhD
Alexandre Pérez-Girbés, MD
Fernando Aparici-Robles, PhD
Ángel Alberich-Bayarri, PhD
Antonio Revert-Ventura, PhD
Luis Martí-Bonmatí, PhD
Juan M. García-Gómez, PhD

Purpose: To determine if preoperative vascular heterogeneity of glioblastoma is predictive of overall survival of patients undergoing standard-of-care treatment by using an unsupervised multiparametric perfusion-based habitat-discovery algorithm.

Materials and Methods: Preoperative magnetic resonance (MR) imaging including dynamic susceptibility-weighted contrast material–enhanced perfusion studies in 50 consecutive patients with glioblastoma were retrieved. Perfusion parameters of glioblastoma were analyzed and used to automatically draw four reproducible habitats that describe the tumor vascular heterogeneity: high-angiogenic and low-angiogenic regions of the enhancing tumor, potentially tumor-infiltrated peripheral edema, and vasogenic edema. Kaplan-Meier and Cox proportional hazard analyses were conducted to assess the prognostic potential of the hemodynamic tissue signature to predict patient survival.

Results: Cox regression analysis yielded a significant correlation between patients' survival and maximum relative cerebral blood volume ($rCBV_{max}$) and maximum relative cerebral blood flow ($rCBF_{max}$) in high-angiogenic and low-angiogenic habitats ($P < .01$, false discovery rate–corrected $P < .05$). Moreover, $rCBF_{max}$ in the potentially tumor-infiltrated peripheral edema habitat was also significantly correlated ($P < .05$, false discovery rate–corrected $P < .05$). Kaplan-Meier analysis demonstrated significant differences between the observed survival of populations divided according to the median of the $rCBV_{max}$ or $rCBF_{max}$ at the high-angiogenic and low-angiogenic habitats (log-rank test $P < .05$, false discovery rate–corrected $P < .05$), with an average survival increase of 230 days.

Conclusion: Preoperative perfusion heterogeneity contains relevant information about overall survival in patients who undergo standard-of-care treatment. The hemodynamic tissue signature method automatically describes this heterogeneity, providing a set of vascular habitats with high prognostic capabilities.

[1] From the Instituto Universitario de Aplicaciones de las Tecnologías de la Información y de las Comunicaciones Avanzadas, Universitat Politècnica de València, Camino de Vera s/n, 46022 Valencia, Spain. Received April 11, 2017; revision requested June 27; revision received September 27; accepted October 10; final version accepted October 27. **Address correspondence to** J.J.A. (e-mail: *jajuaal1@ibime.upv.es*).

Study supported by H2020 European Institute of Innovation and Technology (POC-2016.SPAIN-07) and Universitat Politècnica de València (PAID-10-14). J.J.A., E.F.G., and J.M.G.G. supported by Secretaría de Estado de Investigación, Desarrollo e Innovación (DPI2016-80054-R, TIN2013-43457-R). E.F.G. supported by CaixaImpulse program from Fundació Bancària "la Caixa" (LCF/TR/CI16/10010016). E.F.G and A.A.B. supported by the Universitat Politècnica de València Instituto Investigación Sanitaria de La Fe (C05).

Glioblastoma heterogeneity has been identified as one of the factors responsible for the high aggressiveness of these neoplasms (1) and as a key hallmark to understanding their resistance to effective therapies (2). Molecular characterization of glioblastomas has advanced the understanding of the biology and heterogeneity of these tumors, improving routine diagnosis, prognosis, and response to therapy (3,4). Glioblastoma is characterized by highly infiltrative and deeply invasive behavior (5). Strong vascular proliferation, robust angiogenesis, and extensive microvasculature heterogeneity are major pathologic features that differentiate glioblastomas from low-grade gliomas (6–8). Such factors have been shown to have a direct effect on prognosis (7). Therefore, the early assessment of the highly heterogeneous vascular architecture of glioblastomas could provide powerful information to improve therapeutic decision making.

Dynamic susceptibility contrast material–enhanced (DSC) magnetic resonance (MR) imaging has been used widely to retrieve physiologic information on glioblastoma vasculature (9–11). DSC quantification involves the computation of the hemodynamic indexes obtained from the kinetic analysis of the T2* concentration time curves retrieved from the first pass of an intravenously injected paramagnetic contrast agent (12). Such indexes have demonstrated powerful capabilities for a wide range of applications such as tumor grading (13,14), neovascularization assessment (15,16), early response to treatment assessment (17,18), recurrence versus radionecrosis (19,20) and prediction of clinical outcome (22–23).

Numerous studies have been focused on the analysis of pretreatment perfusion indexes to assess tumor heterogeneity (24–27). A common practice is the manual definition of regions of interest (ROIs) within the tumor. These manual approaches impair the reproducibility of the ROIs and the analysis of multiparametric MR imaging data (28).

The preoperative characterization of the vascular heterogeneity of glioblastomas through a multiparametric search of habitats drawn from an unsupervised machine learning process has not previously been well established in the literature. We hypothesize that the habitats obtained in the preoperative evaluation of glioblastoma are early predictors of overall survival in patients who subsequently undergo standard-of-care treatment.

The hemodynamic tissue signature (HTS) method (29) delineates a set of vascular habitats within the glioblastoma that are obtained through a multiparametric structured clustering of morphologic and DSC MR imaging features. HTS includes consideration of four habitats: the high-angiogenic tumor (the more perfused area of the enhancing tumor), the low-angiogenic tumor (the area of the enhancing tumor with a lower angiogenic profile), the potentially infiltrated peripheral edema (the surrounding nonenhancing region adjacent to the tumor with elevated perfusion indexes), and the vasogenic peripheral edema (the remaining edema with a lower perfusion profile). To determine whether the preoperative vascular heterogeneity of glioblastoma allows early prediction of overall survival of patients who undergo standard-of-care treatment, we conducted a survival analysis on the basis of perfusion measures obtained from the HTS.

Advances in Knowledge

- Preoperative maximum relative cerebral blood volume ($rCBV_{max}$) and maximum relative cerebral blood flow ($rCBV_{max}$) in high-angiogenic and low-angiogenic tumor habitats and $rCBV_{max}$ in the potentially infiltrated peripheral edema habitat of the hemodynamic tissue signature are associated with overall patient survival (Cox regression: $P < .05$, false discovery rate–corrected $P < .05$).
- An increase of 230 days in overall survival was observed for patients with low maximum relative cerebral blood flow in high-angiogenic and low-angiogenic habitats (Kaplan-Meier log-rank test, $P < .05$; false discovery rate–corrected $P < .05$).
- Hemodynamic tissue signatures automatically allow multiparametric reproducible vascular habitats showing tumor heterogeneity (global probabilistic deviation: rCBV = 0.88 ± 0.03; rCBF = 0.86 ± 0.05) to be distinguished in the preoperative evaluation of glioblastomas.

Implication for Patient Care

- Preoperative hemodynamic tissue signature habitats provide early information about expected survival of patients with glioblastoma undergoing standard-of-care treatment.

Materials and Methods

Patient Selection

Our institutional review board approved this retrospective study, and the requirement for patient informed consent was waived. Eighty-four patients from January 2012 to December 2016 with suspected glioblastoma were included. The inclusion criteria were: *(a)* confirmation of

https://doi.org/10.1148/radiol.2017170845

Content codes: MR NR

Radiology 2018; 287:944–954

Abbreviations:

DSC = dynamic susceptibility contrast enhanced
GBCA = gadolinium-based contrast agent
HTS = hemodynamic tissue signature
rCBF = relative cerebral blood flow
$rCBF_{max}$ = maximum rCBF
rCBV = relative cerebral blood volume
$rCBV_{max}$ = maximum rCBV
ROI = region of interest

Author contributions:

Guarantors of integrity of entire study, J.J.A., E.F.G., L.M.B., J.M.G.G.; study concepts/study design or data acquisition or data analysis/interpretation, all authors; manuscript drafting or manuscript revision for important intellectual content, all authors; approval of final version of submitted manuscript, all authors; agrees to ensure any questions related to the work are appropriately resolved, all authors; literature research, J.J.A., E.F.G., A.P.G., F.A.R., A.A.B., A.R.V., J.M.G.G.; clinical studies, J.J.A., E.F.G., F.A.R., A.R.V., L.M.B., J.M.G.G.; experimental studies, J.J.A., E.F.G., A.P.G., F.A.R., J.M.G.G.; statistical analysis, J.J.A., E.F.G., J.M.G.G.; and manuscript editing, J.J.A., E.F.G., A.P.G., F.A.R., A.A.B., L.M.B., J.M.G.G.

Conflicts of interest are listed at the end of this article.

glioblastoma through biopsy; *(b)* access to preoperative MR imaging examinations, including unenhanced and gadolinium-based contrast agent (GBCA)–enhanced T1-weighted, T2-weighted, fluid-attenuated inversion-recovery T2-weighted, and DSC sequences; and *(c)* patients who underwent standard Stupp treatment (30). Of the 84 initial patients, six were excluded because of an incomplete MR imaging study, three were excluded because of motion or spike artifacts on the DSC images that prevented the quantification (gamma variate R^2 goodness of fit < 0.95), 10 patients were excluded because of unconfirmed or unconventional glioblastomas (giant cell glioblastoma and glioblastoma with oligodendroglioma component), and 10 patients were excluded because they did not undergo resection because of their tumor location (only biopsy results available) or they did not undergo radiation therapy and chemotherapy treatment. In addition, five patients who presented with glioblastomas with contiguous leptomeningeal extensions were excluded from the study because of the inability to accurately differentiate the tumor vascularity from the reactive meningeal enhancement in the perfusion signal intensity. Finally, 50 patients constituted the study group, including 33 men with an average age of 60.94 years (range, 25–80 years); 17 women with an average age of 62.53 years (range, 36–75 years); and an overall mean age of 60.08 years (range, 25–80 years).

MR Imaging

Standard-of-care examinations were obtained with 1.5-T or 3-T imagers (Signa HDxt; GE Healthcare, Waukesha, Wis) with an eight-channel-array head coil. MR imaging examinations included unenhanced and GBCA–enhanced T1-weighted three-dimensional spoiled gradient-echo sequences with inversion recovery (repetition times msec/echo times msec, 6–10/2–4; matrix, 256 × 256; section thickness, 1.5 mm; field of view, 24 × 24 cm; inversion time, 400 msec; flip angle, 70°–80°), fast spin-echo T2-weighted imaging (3000–4000/100–110; matrix, 256 × 256; section thickness, 5 mm; field of view, 21.9 × 21.9 cm; one signal acquired; intersection gap, 2 mm) and a fluid-attenuated inversion-recovery T2-weighted sequence (8000–9000/140–165; matrix, 256 × 192; section thickness, 5 mm; field of view, 22 × 22 cm; one signal acquired; intersection gap, 2 mm; inversion time, 2.200 msec).

The DSC T2*-weighted gradient-echo perfusion study was performed during the injection of GBCA (Multihance; Bracco, Milan, Italy). A bolus injection of 0.1 mmol/kg of GBCA was administered at 5 mL/sec by using a power injector (no prebolus administration). Saline solution was injected after the bolus injection. The study was performed with the following parameters: 2000/25; matrix, 128 × 128 (1.8 × 1.8 mm in-plane resolution); section thickness, 7 mm; flip angle, 60°; 14 cm full-coverage cranio-caudal (20 sections), 40 sequential temporally equidistant volumes, each one with an acquisition time of 2 seconds. The baseline before injection of the bolus was five dynamics.

Quantification of DSC Parametric Maps

Registration of the DSC T2*-weighted sequence was first conducted to the morphologic T2-weighted image of the patient. Relative cerebral blood volume (rCBV) and relative cerebral blood flow (rCBF) maps were obtained with standard algorithms previously described (31). First, signal intensity curves were converted to concentration time curves by using the following equation:

$$\Delta R2^{*}(t) = -\ln\left(\frac{\mathrm{SI}(t)}{\mathrm{SI}_0}\right)/\mathrm{TE},$$

where SI (t) is the T2* signal intensity at time t, SI_0 is the unenhanced baseline signal intensity of SI, and TE is the echo time. Contrast material leakage correction was performed by using the technique proposed by Boxerman et al (32) and by means of gamma-variate curve fitting. rCBV was computed according to numerical integration of the area under the curve of the gamma-variate fittings (31); while rCBF was calculated by means of the block-circulant singular value decomposition deconvolution scheme proposed in Wu et al (33). Both perfusion maps were normalized against the contralateral unaffected white matter value. The arterial input function was automatically selected by following a divide-and-conquer approach. The method recursively dichotomizes the set of concentration time curves of the perfusion study into two groups, selecting those curves with higher peak height, earliest time to peak, and lowest full-width at half maximum. We used the median as a threshold to split the groups. The process is repeated until 10 or fewer curves are conserved, finally fixing the arterial input function as the average of those curves.

Enhancing Tumor and Edema ROI Segmentation

Enhancing tumor and edema ROI delineation was performed by using an unsupervised segmentation method based on a variant of the work proposed in a study by Juan-Albarracín (34). This method is based on Directional Class Adaptive Spatially Varying Finite Mixture Model, or DCA-SVFMM (35), which consists of a clustering algorithm that combines Gaussian mixture modeling with continuous Markov random fields to take advantage of the self-similarity and local redundancy of the images. The method includes the unenhanced and GBCA–enhanced T1-weighted sequences, the T2-weighted sequence, and the fluid-attenuated inversion-recovery T2-weighted sequence in combination with atlas-based prior knowledge of healthy tissues to perform the segmentation. The automated enhancing tumor and edema ROIs obtained with the method were manually revised and validated by two experienced radiologists in consensus (F.A., with 14 years of experience; L.M.B., with 25 years of experience).

HTS Habitats

The HTS consists of a set of vascular habitats detected in glioblastomas and obtained by means of a multiparametric unsupervised analysis of DSC MR imaging patterns within the tumor. The technology used to compute the HTS of the glioblastoma was introduced by Juan-Albarracín (29) and is publicly accessible for noncommercial research purposes at *https://www.oncohabitats.upv.es*. The

HTS defines four habitats within the glioblastoma: the high- and low-angiogenic enhancing tumor habitats, and the infiltrated peripheral edema and vasogenic peripheral edema habitats. Table 1 summarizes the relationships among HTS habitats, glioblastoma tissue, and DSC observed vascularity.

HTS habitats were obtained by means of a DCA-SVFMM structured clustering of rCBV and rCBF maps. The clustering consists of two stages (Fig 1): *(a)* a two-class clustering of the whole enhancing tumor and edema ROIs and *(b)* a two-class clustering performed by using only the rCBV and rCBF data within the ROIs obtained in stage a. To ensure the reproducibility of the HTS, both stages were initialized with a deterministic seed method. We fixed the seeds of every two-class clustering to the extremes of the rCBV and rCBV distributions (5% and 95% percentiles, respectively, for each class).

The aim of the first stage was to refine the enhancing tumor and the edema ROI previously delineated through the morphologic MR imaging introducing the perfusion information. Hence, a spatially varying mixture of two Gaussians was fit to the distributions of rCBV and rCBF observed in this ROI. We named these two classes enhancing tumor at DSC and edema at DSC, respectively. During the fitting process, we introduced several constraints to avoid misclassifications of nearby healthy vascular structures. We constrained the apparition of the enhancing tumor at DSC class to a neighborhood of less than 1 cm around the enhancing tumor observed on the GBCA–enhanced T1-weighted MR images (36). This constraint allowed the correction of misalignments during the DSC registration and the removal of healthy vascular structures far from the enhancing area of the tumor, which may distort the HTS.

The second stage included DCA-SVFMM clustering within the enhancing tumor at DSC and edema at DSC ROIs to delineate the two potential hemodynamic habitats inside each tissue. Likewise, the first stage, a spatially varying mixture of two Gaussians was fit to the distributions of rCBV and rCBF for both the enhancing tumor and edema at DSC ROIs. In this stage, several constraints were also introduced. First, we forced a minimum size of the habitats of at least 10% of the whole lesion ROI to avoid habitat vanishing. Second, infiltrated peripheral edema habitat was also constrained to a nearby region around the enhancing tumor at DSC class. Following the definition of the clinical target volume proposed in Guo et al (36), we fixed a 2-cm margin around the enhancing tumor observed at GBCA-enhanced T1-weighted MR imaging as the maximum

Table 1

Glioblastoma Hemodynamic Habitats Considered by the HTS

HTS Habitat	Vascularity	Glioblastoma-related Tissue
High angiogenic	Highest	High-angiogenic enhancing tumor
Low angiogenic	High	Low-angiogenic enhancing tumor
Infiltrated peripheral edema	Low	Potentially tumor infiltrated peripheral edema
Vasogenic peripheral edema	Lowest	Vasogenic peripheral edema

Figure 1

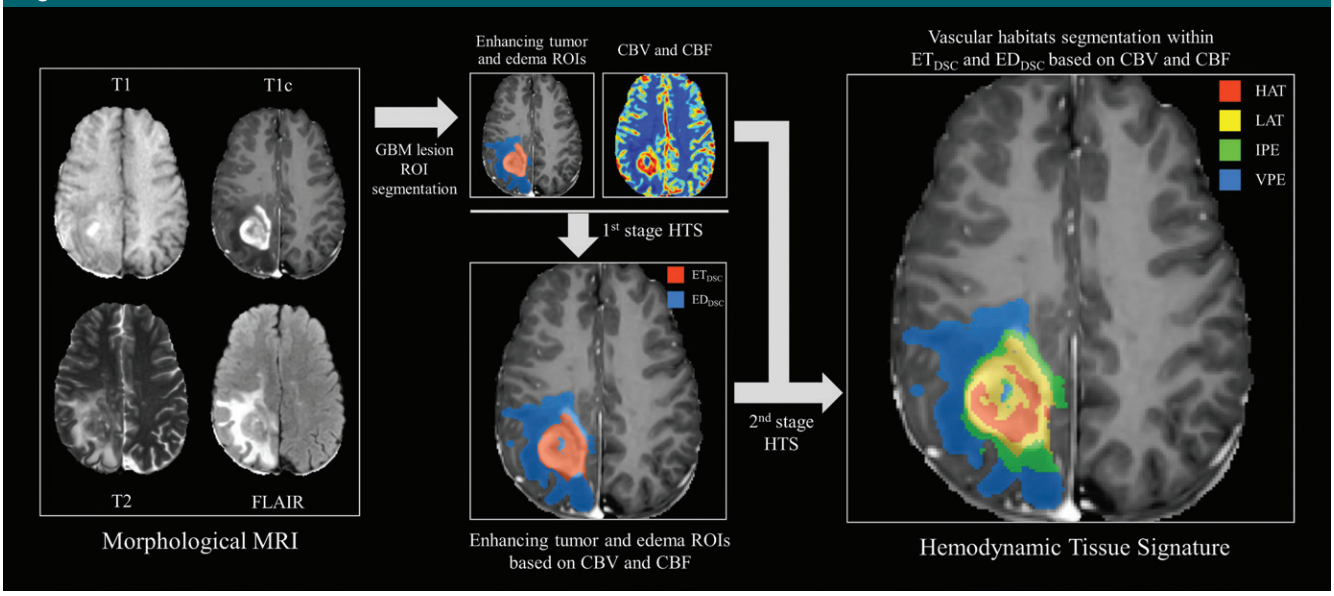

Figure 1: Schema of the methodology used to compute the HTS of the glioblastoma. ED_{DSC} = edema at DSC, ET_{DSC} = enhancing tumor at DSC, *HAT* = high-angiogenic tumor; *LAT* = low-angiogenic tumor, *IPE* = infiltrated peripheral edema, *VPE* = vasogenic peripheral edema, *T1c* = T1-weighted contrast enhanced.

Figure 2

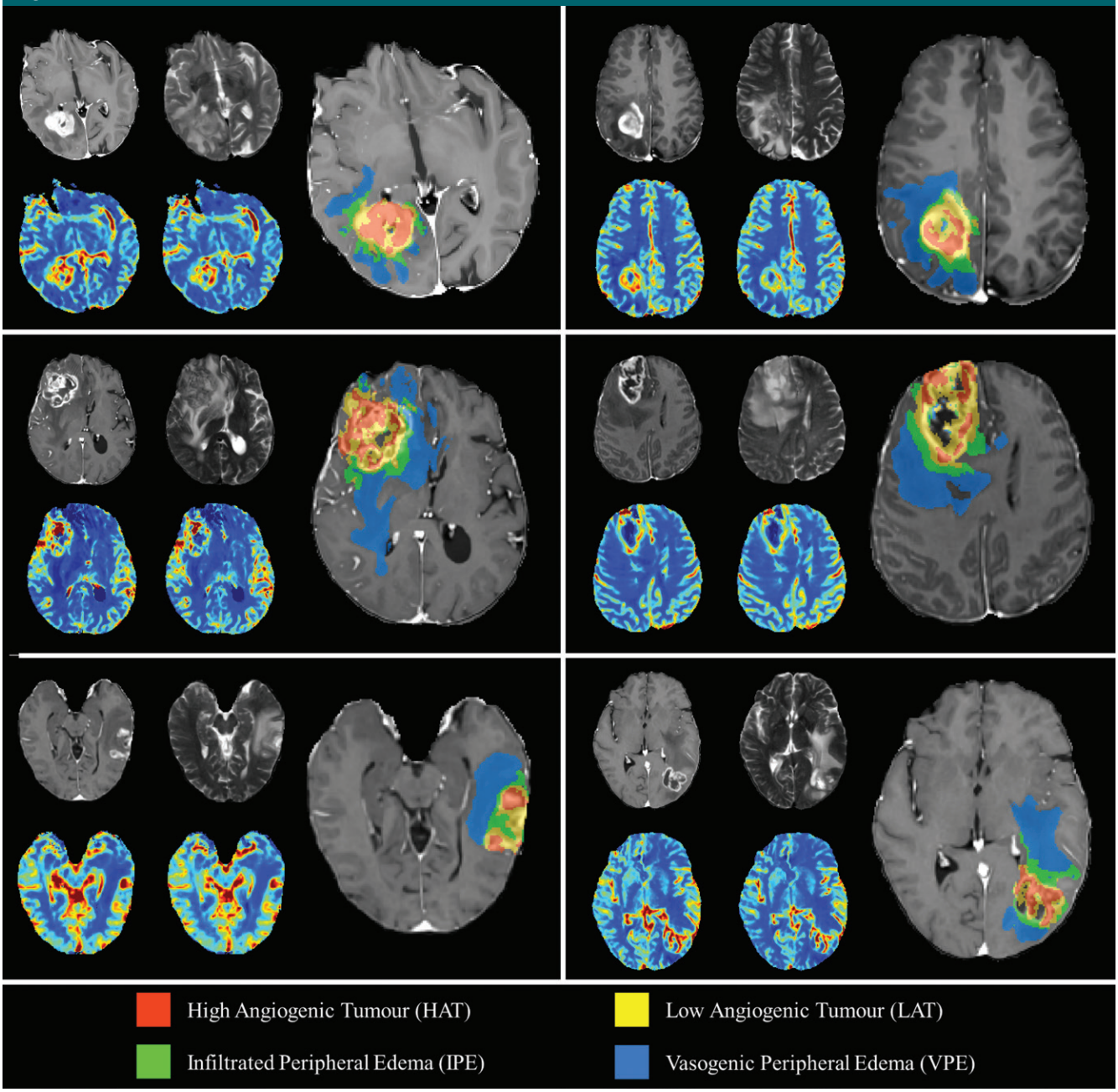

Figure 2: Examples of the HTS habitat's map placed over the GBCA-enhanced T1-weighted MR image for six patients. In addition, for each patient, GBCA-enhanced T1-weighted MR image, T2-weighted MR image, CBV map, CBF map, are also shown in small images (left to right, top to bottom).

distance where the infiltrated peripheral edema habitat could appear. Voxels classified as infiltrated peripheral edema outside this region were automatically removed from the HTS, because they have a similar vascular pattern to that of infiltrated peripheral edema but far from the plausible region of tumor infiltration.

Statistical Analysis

All analyses were performed with software (Matlab R2015a; MathWorks, Natick, Mass) on a personal workstation. First, an evaluation of the statistical differences between habitats was conducted to assess the degree of separability of the rCBV and rCBF distributions within each habitat to confirm their different hemodynamic activity. To do so, global probabilistic deviation (37) was

used as a metric to control the degree of concordance among several statistical distributions. Such a metric is bounded to a 0–1 range, with 0 referring to absolute overlapping between distributions, and 1 indicating nonoverlapped, completely separated distributions. Therefore, for each perfusion parameter, the distributions of the four proposed habitats and their global probabilistic deviation metric were calculated.

Second, Cox proportional hazards modeling was conducted to investigate the relationship between patient survival and the $rCBV_{max}$ and $rCBF_{max}$ at the HTS habitats. We used the maximum of the perfusion parameters because it has been reported to be the most reliable measure for interobserver and intraobserver reproducibility (38). Proportional hazard ratios with 95% confidence intervals were reported, while the Wald test was used to determine the significance of the Cox regression model results.

Finally, Kaplan-Meier survival analyses between populations dichotomized according to the median value of each perfusion biomarker at each HTS habitat were also conducted. A log-rank test was used to determine the statistical significance of the differences in observed population survival. Average survival for each population was also reported. Benjamini-Hochberg false discovery rate correction at an α level of .05 was used to correct for multiple hypothesis testing (39) in all analyses.

Results

Figure 2 shows examples of HTS maps. GBCA-enhanced T1-weighted and T2-weighted images, as well as rCBV and rCBF maps are shown with the HTS map of the patient. The global probabilistic deviation analysis of the different hemodynamic activity among habitats yielded the following average results: 0.88 ± 0.03 for rCBV and 0.86 ± 0.05 for rCBF. These results indicate separated perfusion distributions between habitats of the patients. Figure 3 shows an example of the rCBV distributions for each HTS habitat.

The Cox proportional hazard analysis is presented in Table 2. Significant results were obtained for $rCBV_{max}$ and $rCBF_{max}$ in the high-angiogenic habitat (hazard ratios, 1.22 [P = .0004] and 1.20 [P = .0004], respectively), $rCBV_{max}$ and $rCBF_{max}$ in the low-angiogenic habitat (hazard ratios, 1.62 [P = .0001] and 1.89 [P = .0005], respectively) and $rCBV_{max}$ in the infiltrated peripheral edema habitat (hazard ratio, 1.67; P = .498). Nonsignificant results were obtained for $rCBF_{max}$ in the infiltrated peripheral edema (hazard ratio, 2.07; P = .0579), and $rCBV_{max}$ in the vasogenic peripheral edema habitat (hazard ratio, 1.59; P = .0962) and $rCBF_{max}$ at vasogenic peripheral edema (hazard ratio, 1.58; P = .2657). Figure 4 shows the scatterplots of the combinations of perfusion biomarkers

Figure 3

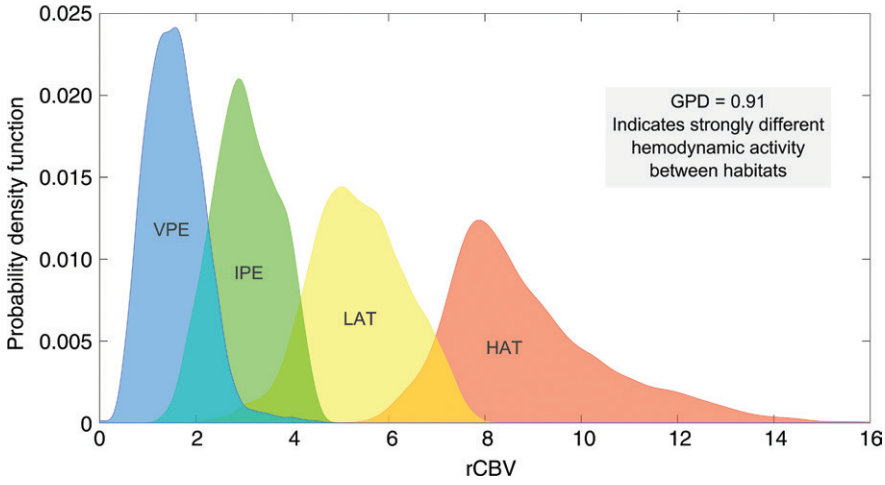

Figure 3: Example of the rCBV distributions at each HTS habitat for a 62-year-old man and the global probabilistic deviation score obtained in the assessment of the separability of the distribution of the habitats. *HAT* = high-angiogenic tumor, *IPE* = infiltrated peripheral edema, *LAT* = low-angiogenic tumor, *VPE* = vasogenic peripheral edema.

Table 2

Cox Proportional Hazard Analysis for Maximum Perfusion Indexes at the HTS Habitats to Predict Patient's Overall Survival

Habitat and Perfusion Indexes	Hazard Ratio	*P* Value*
High-angiogenic tumor		
$rCBV_{max}$	1.22 (1.10, 1.35)	.0004†
$rCBF_{max}$	1.20 (1.09, 1.32)	.0004†
Low-angiogenic tumor		
$rCBV_{max}$	1.62 (1.31, 2.01)	.0001†
$rCBF_{max}$	1.89 (1.35, 2.66)	.0005†
Infiltrated peripheral edema		
$rCBV_{max}$	1.67 (1.05, 2.66)	.0498†
$rCBF_{max}$	2.07 (1.02, 4.20)	.0579
Vasogenic peripheral edema		
$rCBV_{max}$	1.59 (0.94, 2.70)	.0962
$rCBF_{max}$	1.58 (0.71, 3.54)	.2657

Note.—Data in parentheses are 95% confidence intervals.

* False discovery rate corrected.

† Indicates a significant difference.

Figure 4

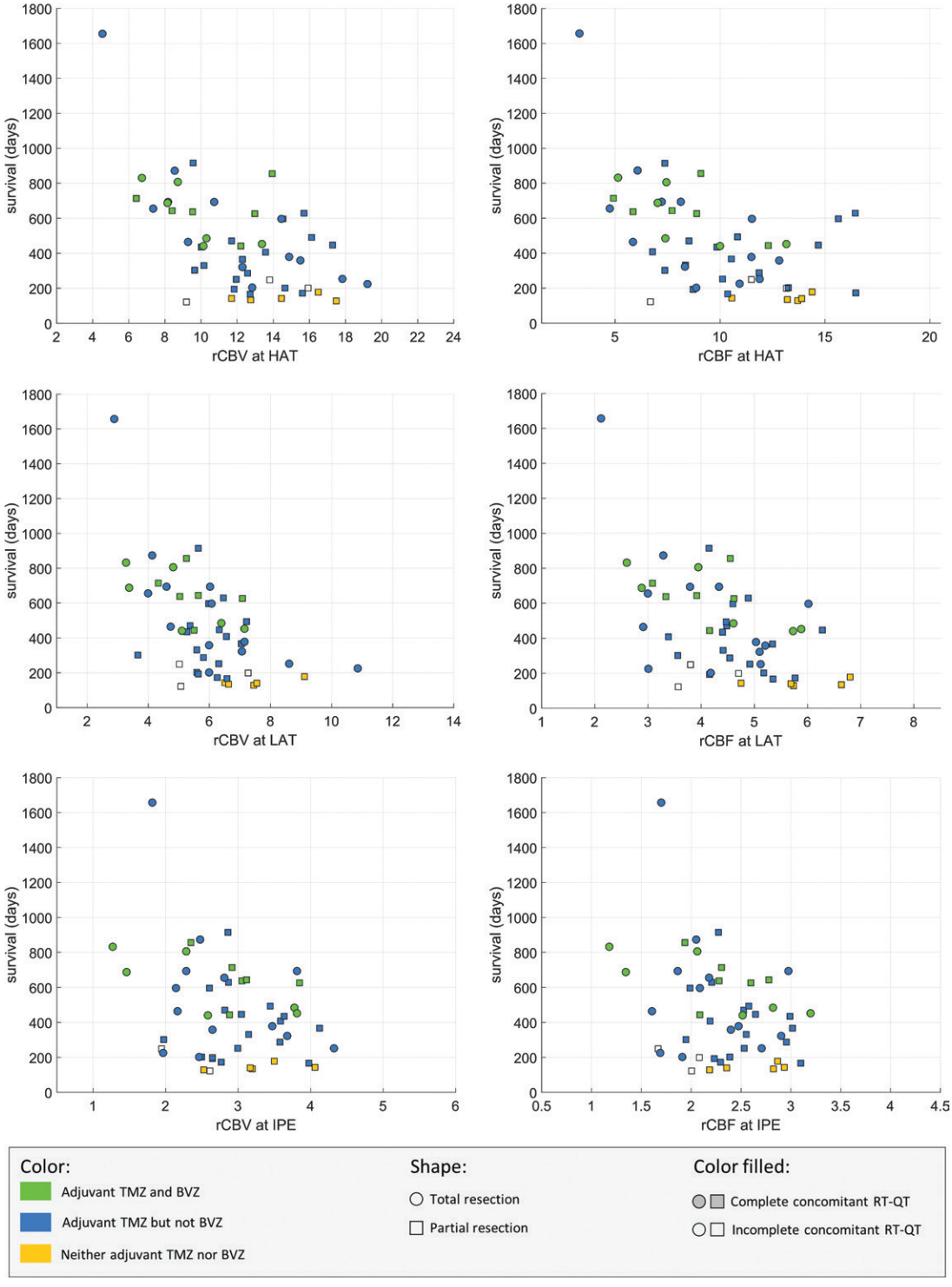

Figure 4: Scatterplots of the relation between patient survival and perfusion biomarkers in high-angiogenic tumor *(HAT)*, low-angiogenic tumor *(LAT)* and inflitrated peripheral edema *(IPE)* habitats. Treatment undergone by each patient is also shown, to allow differentiation between total versus partial resection, complete versus incomplete concomitant radiation therapy and chemotherapy, adjuvant temozolomide and bevacizumab administration. *BVZ* = bevacizumab, *RT-QT* = radiation therapy-chemotherapy, *TMZ* = temozolomide.

and HTS habitats that yielded significant correlation in the Cox survival analysis. Total versus partial maximum safe resection, complete versus incomplete concomitant radiation therapy and chemotherapy and adjuvant temozolomide plus bevacizumab administration are also shown.

Kaplan-Meier survival analysis yielded significant differences for the survival times observed for the populations dichotomized by low and high $rCBV_{max}$ in the high-angiogenic habitat (log-rank test $P = .0104$), $rCBF_{max}$ in the high-angiogenic habitat (log-rank test $P = .0003$), $rCBV_{max}$ at low-angiogenic habitat (log-rank test $P = .0048$) and $rCBF_{max}$ in the low-angiogenic habitat (log-rank test $P = .0128$). An average difference of 230 days in overall survival between populations was observed. Mean survival of the population was 459 days ± 286.15 (range, 121–1656 days). Table 3 shows the average observed survival times for each population and the corrected *P* values for the log-rank survival test. Figure 5 demonstrates the Kaplan-Meier estimated survival functions for the different populations dichotomized according to the $rCBV_{max}$ and $rCBF_{max}$ at different HTS habitats.

Table 3

Kaplan-Meier Survival Analysis for Populations with High versus Low Maximum Perfusion Parameters at the Different Habitats

Habitat and Perfusion Parameter	Average Survival (days)		*P* Value*
	Low	High	
High-angiogenic tumor			
$rCBV_{max}$	550.33	351.78	.0104†
$rCBF_{max}$	594.73	311.96	.0003†
Low-angiogenic tumor			
$rCBV_{max}$	571.62	337	.0048†
$rCBF_{max}$	554.96	355.04	.0128†
Infiltrated peripheral edema			
$rCBV_{max}$	500.52	423.63	.7986
$rCBF_{max}$	557.17	368.38	.0641
Vasogenic peripheral edema			
$rCBV_{max}$	532.56	385.44	.1300
$rCBF_{max}$	500.92	420.31	.8992

Note.—Median value for the vascular parameter at each HTS was used to divide the population.

* False discovery rate corrected.

† Indicates a significant difference.

Discussion

In this study, we investigated whether the perfusion heterogeneity in the four vascular habitats of the HTS is predictive of survival in untreated glioblastomas. Our results demonstrate that the preoperative perfusion heterogeneity contains relevant information about patient survival, even considering the effect of other known relevant factors such as standard-of-care treatment. Gradually longer survival times were found for patients who presented with lower preoperative perfusion indexes in different HTS habitats. The influence of standard-of-care treatment on patient survival was also directly observed. As expected, patients who underwent maximal safe resection plus concomitant adjuvant chemotherapy and radiation therapy showed better survival times. However, a tendency of longer survival times within subgroups of patients who underwent the same specific treatment and had lower perfusion indexes at several habitats was also observed. This indicates that preoperative perfusion heterogeneity contains early important information about patient survival.

Cox proportional hazard analysis substantiated these conclusions. High- and low-angiogenic habitats arose as those with the highest prognostic abilities, yielding significant correlations between survival and $rCBV_{max}$ and $rCBF_{max}$ (with multiple-test false discovery rate correction). $rCBV_{max}$ in the infiltrated peripheral edema habitat also was significantly correlated with survival, while $rCBF_{max}$ in the infiltrated peripheral edema was significantly correlated without multiple-test correction ($P = .0434$). These results suggest that relevant information about patient survival is also contained in the peripheral edema (23,40,41).

Significant differences also were observed in the Kaplan-Meier estimated survival functions for populations divided according to the median $rCBV_{max}$ and $rCBF_{max}$ at several HTS habitats. An improvement of approximately 230 days in overall survival was observed for patients who had lower $rCBV_{max}$ and $rCBF_{max}$ in the high- and low-angiogenic habitats. These results support the potential of HTS to accurately describe the preoperative vascular heterogeneity of glioblastomas and its prognostic abilities at early stages.

Several studies have been conducted to analyze the vascular heterogeneity of the glioblastoma, many of them focusing on the enhancing tumor region. Law et al (21) found that patients who presented with an $rCBV_{max}$ of less than 1.75 in the enhancing tumor had longer progression-free survival times; however, they did not find a significant correlation with overall survival. Sawlani et al (42) also correlated time to progression with several hyperperfused regions delineated in the rCBV. However, they also observed no significant correlation between patients' overall survival and $rCBV_{max}$ in the enhancing tumor. Hirai et al (43) and Jain et al (44), studied the potential for prediction of survival of rCBV in the enhancing tumor of high-grade gliomas. They showed that patients who presented with an $rCBV_{max}$ of greater than 2.3 had significantly shorter survival times. These results are consistent with our findings, hence aligning HTS with the results of previous studies in the literature. However, these

Figure 5

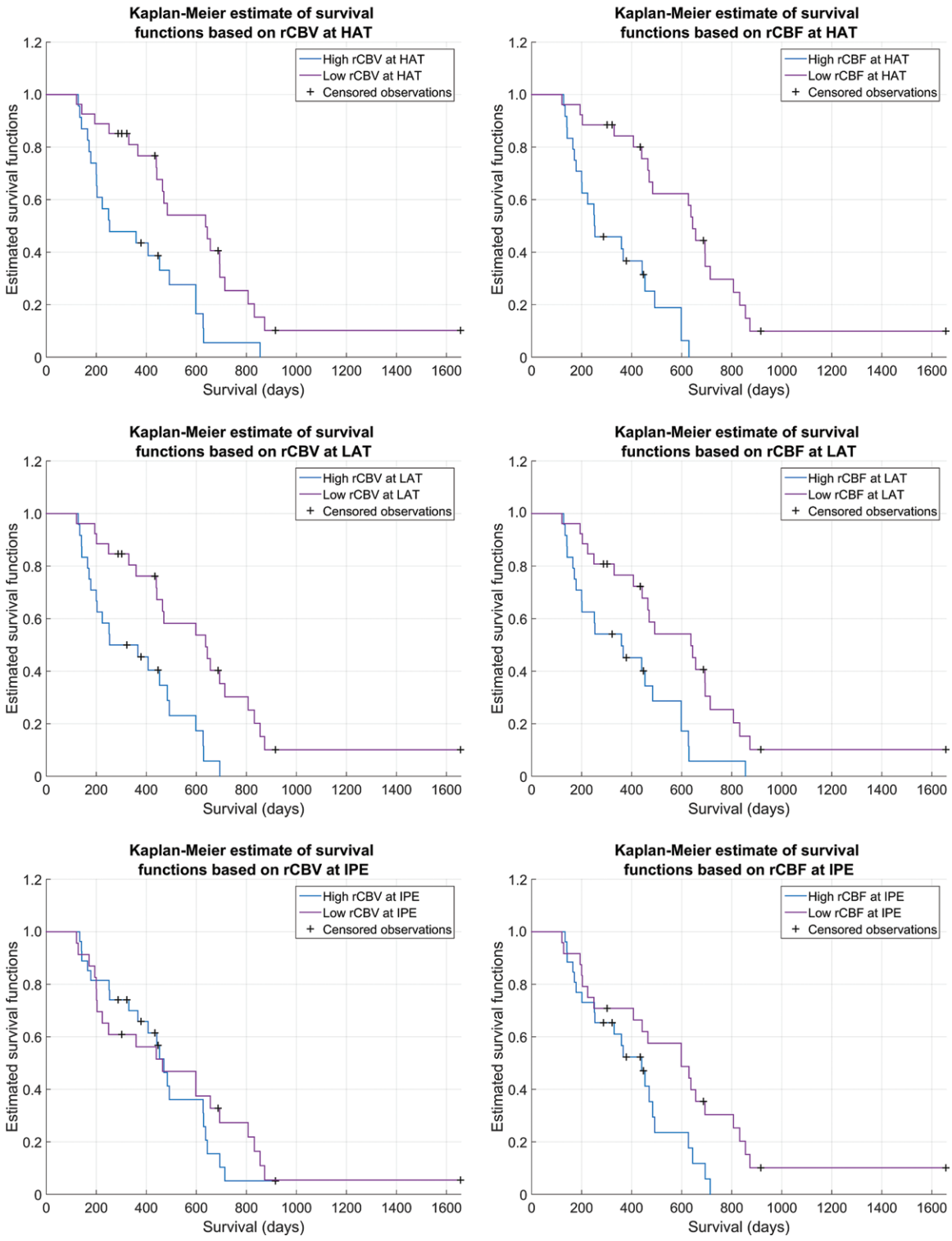

Figure 5: Kaplan-Meier estimated survival functions for the populations divided by the median $rCBV_{max}$ or $rCBF_{max}$ in high-angiogenic tumor *(HAT)*, low-angiogenic tumor *(LAT)* and inflitrated peripheral edema *(IPE)* habitats.

studies were only based on the $rCBV_{max}$; other perfusion indexes such as $rCBF_{max}$, which may also add important information about instantaneous capillary flow in the tissues to the analysis, were not considered. Moreover, manual delineation of ROIs based on $rCBV_{max}$ was used, which may affect reproducibility and may not fully capture the tumor information available in a multiparametric study.

Authors of other studies focused on peripheral edema of glioblastoma. Akbari et al (40), Jain et al (23) and Arzti et al (41) studied the peritumoral region of the glioblastoma to account for heterogeneity and possible tumor infiltration in the peripheral edema. Akbari et al used ROIs to train a support vector machine, which was then used to generate heterogeneity maps. Jain et al analyzed the association of Visually Accessible Rembrandt Images, or VASARI, features and molecular data with overall survival and progression-free survival, while Artzi et al used diffusion, perfusion, and morphologic MR imaging with an unsupervised segmentation algorithm to analyze the edema region. Their results correlate with our findings in the infiltrated peripheral edema habitat, because they also found that vascular heterogeneity in the peripheral edema correlate with overall patient survival. However, ROIs to describe tumor heterogeneity in these studies were also delineated manually. Moreover, statistical tests were conducted without multiple comparison correction, which decreases the statistical power of the conclusions.

One of the main limitations of our study and similar studies in which authors attempted to describe the vascular heterogeneity of glioblastoma by means of discovery of new habitats was the unavailability of a ground truth for validating the habitat's segmentation (40,43,44). Multiple biopsy or pathologic sampling could confirm the accuracy of the habitats; however, such techniques cannot always be performed in clinical practice. To overcome this limitation, alternative validation should be conducted to demonstrate the clinical relevance of the habitats. In this study, we have analyzed the relationship between the preoperative vascular heterogeneity of glioblastomas described through HTS and patient survival.

Another important limitation was the lack of molecular markers in the population of our study. Molecular markers are currently considered a standard of care for World Health Organization glioblastoma classification and are also known to affect prognosis of patients with glioblastoma. Positive correlation of genetic markers with the HTS habitats would strengthen the study and the predictive potential of the proposed method and should be performed in the future.

Finally, a limitation of the HTS arises in the presence of highly vascularized healthy structures close to the glioblastoma, such as nearby vessels or arteries. In such cases, these structures can be misidentified as high- and low-angiogenic or infiltrated peripheral edema habitats depending on their degree of vascularity. Although HTS implements several constraints to remove these healthy structures, nearby vessels may influence the HTS, modifying measures obtained from the habitats. Results of future studies should improve vessel detection by using a vascular probability atlas to weight the HTS inference process.

In conclusion, preoperative vascular heterogeneity of glioblastomas demonstrated by the habitats of HTS is associated with patient survival. HTS separates glioblastomas into four vascular habitats with early prognostic capabilities, offering an opportunity to define refined imaging biomarkers surrogated to clinical outcomes.

Disclosures of Conflicts of Interest: J.J.A. Activities related to the present article: disclosed no relevant relationships. Activities not related to the present article: disclosed no relevant relationships. Other relationships: patent (P201431289) issued. **E.F.G.** Activities related to the present article: disclosed no relevant relationships. Activities not related to the present article: disclosed no relevant relationships. Other relationships: patent issued (P201431289). **A.P.G.** Activities related to the present article: grant from Bracco. Activities not related to the present article: disclosed no relevant relationships. Other relationships: disclosed no relevant relationships. **F.A.R.** disclosed no relevant relationships. **A.A.B.** Activities related to the present article: disclosed no relevant relationships. Activities not related to the present article: employment with and stock options for Quibim SL. Other relationships: disclosed no relevant relationships. **A.R.V.** disclosed no relevant relationships. **L.M.B.** disclosed no relevant relationships. **J.M.G.G.** Activities related to the present article: disclosed no relevant relationships. Activities not related to the present article: disclosed no relevant relationships. Other relationships: patent issued (P201431289).

References

1. Lemée JM, Clavreul A, Menei P. Intratumoral heterogeneity in glioblastoma: don't forget the peritumoral brain zone. Neuro Oncol 2015;17(10):1322–1332.
2. Soeda A, Hara A, Kunisada T, Yoshimura S, Iwama T, Park DM. The evidence of glioblastoma heterogeneity. Sci Rep 2015;5(1):7979 [Published correction appears in Sci Rep 2015;5:9630.].
3. Parsons DW, Jones S, Zhang X, et al. An integrated genomic analysis of human glioblastoma multiforme. Science 2008;321(5897):1807–1812.
4. Verhaak RG, Hoadley KA, Purdom E, et al. Integrated genomic analysis identifies clinically relevant subtypes of glioblastoma characterized by abnormalities in PDGFRA, IDH1, EGFR, and NF1. Cancer Cell 2010;17(1):98–110.
5. Dang L, Jin S, Su SM. IDH mutations in glioma and acute myeloid leukemia. Trends Mol Med 2010;16(9):387–397.
6. Alves TR, Lima FR, Kahn SA, et al. Glioblastoma cells: a heterogeneous and fatal tumor interacting with the parenchyma. Life Sci 2011;89(15-16):532–539.
7. Hardee ME, Zagzag D. Mechanisms of glioma-associated neovascularization. Am J Pathol 2012;181(4):1126–1141.
8. Kargiotis O, Rao JS, Kyritsis AP. Mechanisms of angiogenesis in gliomas. J Neurooncol 2006;78(3):281–293.
9. Shah MK, Shin W, Parikh VS, et al. Quantitative cerebral MR perfusion imaging: preliminary results in stroke. J Magn Reson Imaging 2010;32(4):796–802.
10. Knopp EA, Cha S, Johnson G, et al. Glial neoplasms: dynamic contrast-enhanced T2*-weighted MR imaging. Radiology 1999;211(3):791–798.
11. Lupo JM, Cha S, Chang SM, Nelson SJ. Dynamic susceptibility-weighted perfusion imaging of high-grade gliomas: characterization of spatial heterogeneity. AJNR Am J Neuroradiol 2005;26(6):1446–1454.
12. Østergaard L. Principles of cerebral perfusion imaging by bolus tracking. J Magn Reson Imaging 2005;22(6):710–717.
13. Law M, Yang S, Wang H, et al. Glioma grading: sensitivity, specificity, and predictive values of perfusion MR imaging and proton

MR spectroscopic imaging compared with conventional MR imaging. AJNR Am J Neuroradiol 2003;24(10):1989–1998.

14. Emblem KE, Nedregaard B, Nome T, et al. Glioma grading by using histogram analysis of blood volume heterogeneity from MR-derived cerebral blood volume maps. Radiology 2008;247(3):808–817.

15. Thompson G, Mills SJ, Coope DJ, O'Connor JP, Jackson A. Imaging biomarkers of angiogenesis and the microvascular environment in cerebral tumours. Br J Radiol 2011; 84(Spec No 2):S127–S144.

16. Tykocinski ES, Grant RA, Kapoor GS, et al. Use of magnetic perfusion-weighted imaging to determine epidermal growth factor receptor variant III expression in glioblastoma. Neuro Oncol 2012;14(5):613–623.

17. Vidiri A, Pace A, Fabi A, et al. Early perfusion changes in patients with recurrent high-grade brain tumor treated with Bevacizumab: preliminary results by a quantitative evaluation. J Exp Clin Cancer Res 2012;31(1):33.

18. Elmghirbi R, Nagaraja TN, Brown SL, et al. Acute Temporal Changes of MRI-Tracked Tumor Vascular Parameters after Combined Anti-angiogenic and Radiation Treatments in a Rat Glioma Model: Identifying Signatures of Synergism. Radiat Res 2017;187(1):79–88.

19. Hu LS, Baxter LC, Smith KA, et al. Relative cerebral blood volume values to differentiate high-grade glioma recurrence from posttreatment radiation effect: direct correlation between image-guided tissue histopathology and localized dynamic susceptibility-weighted contrast-enhanced perfusion MR imaging measurements. AJNR Am J Neuroradiol 2009;30(3):552–558.

20. Barajas RF, Chang JS, Sneed PK, Segal MR, McDermott MW, Cha S. Distinguishing recurrent intra-axial metastatic tumor from radiation necrosis following gamma knife radiosurgery using dynamic susceptibility-weighted contrast-enhanced perfusion MR imaging. AJNR Am J Neuroradiol 2009;30(2):367–372.

21. Law M, Young RJ, Babb JS, et al. Gliomas: predicting time to progression or survival with cerebral blood volume measurements at dynamic susceptibility-weighted contrast-enhanced perfusion MR imaging. Radiology 2008;247(2):490–498.

22. Mangla R, Singh G, Ziegelitz D, et al. Changes in relative cerebral blood volume 1 month after radiation-temozolomide therapy can help predict overall survival in patients with glioblastoma. Radiology 2010;256(2):575–584.

23. Jain R, Poisson LM, Gutman D, et al. Outcome prediction in patients with glioblastoma by using imaging, clinical, and genomic biomarkers: focus on the nonenhancing component of the tumor. Radiology 2014;272(2):484–493.

24. Jackson A, O'Connor JP, Parker GJ, Jayson GC. Imaging tumor vascular heterogeneity and angiogenesis using dynamic contrast-enhanced magnetic resonance imaging. Clin Cancer Res 2007;13(12):3449–3459.

25. Liu TT, Achrol AS, Mitchell LA, et al. Magnetic resonance perfusion image features uncover an angiogenic subgroup of glioblastoma patients with poor survival and better response to antiangiogenic treatment. Neuro Oncol 2017;19(7):997–1007.

26. Sanz-Requena R, Revert-Ventura A, Martí-Bonmatí L, Alberich-Bayarri A, García-Martí G. Quantitative MR perfusion parameters related to survival time in high-grade gliomas. Eur Radiol 2013;23(12):3456–3465.

27. Ulyte A, Katsaros VK, Liouta E, et al. Prognostic value of preoperative dynamic contrast-enhanced MRI perfusion parameters for high-grade glioma patients. Neuroradiology 2016;58(12):1197–1208.

28. Young R, Babb J, Law M, Pollack E, Johnson G. Comparison of region-of-interest analysis with three different histogram analysis methods in the determination of perfusion metrics in patients with brain gliomas. J Magn Reson Imaging 2007;26(4):1053–1063.

29. Juan-Albarracín J, Fuster-Garcia E, Garcia-Gomez JM. An online platform for the automatic reporting of multi-parametric tissue signatures: A case study in Glioblastoma. In 2nd International Workshop: Brainlesion: Glioma, Multiple Sclerosis, Stroke and Traumatic Brain Injuries. 19th International Conference on Medical Image Computing and Computer Assisted Intervention (MICCAI) 2016. Lecture Notes in Computer Science, vol 9968. Springer..

30. Stupp R, Mason WP, van den Bent MJ, et al. Radiotherapy plus concomitant and adjuvant temozolomide for glioblastoma. N Engl J Med 2005;352(10):987–996.

31. Knutsson L, Ståhlberg F, Wirestam R. Absolute quantification of perfusion using dynamic susceptibility contrast MRI: pitfalls and possibilities. MAGMA 2010;23(1):1–21.

32. Boxerman JL, Schmainda KM, Weisskoff RM. Relative cerebral blood volume maps corrected for contrast agent extravasation significantly correlate with glioma tumor grade, whereas uncorrected maps do not. AJNR Am J Neuroradiol 2006;27(4):859–867.

33. Wu O, Østergaard L, Weisskoff RM, Benner T, Rosen BR, Sorensen AG. Tracer arrival timing-insensitive technique for estimating flow in MR perfusion-weighted imaging using singular value decomposition with a block-circulant deconvolution matrix. Magn Reson Med 2003;50(1):164–174.

34. Juan-Albarracín J, Fuster-Garcia E, Manjón JV, et al. Automated glioblastoma segmentation based on a multiparametric structured unsupervised classification. PLoS One 2015;10(5):e0125143.

35. Nikou C, Galatsanos NP, Likas AC. A class-adaptive spatially variant mixture model for image segmentation. IEEE Trans Image Process 2007;16(4):1121–1130.

36. Guo L, Wang G, Feng Y, et al. Diffusion and perfusion weighted magnetic resonance imaging for tumor volume definition in radiotherapy of brain tumors. Radiat Oncol 2016;11(1):123.

37. Sáez C, Robles M, García-Gómez JM. Stability metrics for multi-source biomedical data based on simplicial projections from probability distribution distances. Stat Methods Med Res 2017;26(1):312–336.

38. Wetzel SG, Cha S, Johnson G, et al. Relative cerebral blood volume measurements in intracranial mass lesions: interobserver and intraobserver reproducibility study. Radiology 2002;224(3):797–803.

39. Benjamini Y, Hochberg Y. Controlling the False Discovery Rate: A Practical and Powerful Approach to Multiple Testing. J R Stat Soc Ser B Methodol 1995;57(1):289–300.

40. Akbari H, Macyszyn L, Da X, et al. Pattern analysis of dynamic susceptibility contrast-enhanced MR imaging demonstrates peritumoral tissue heterogeneity. Radiology 2014;273(2):502–510.

41. Artzi M, Bokstein F, Blumenthal DT, et al. Differentiation between vasogenic-edema versus tumor-infiltrative area in patients with glioblastoma during bevacizumab therapy: a longitudinal MRI study. Eur J Radiol 2014;83(7):1250–1256.

42. Sawlani RN, Raizer J, Horowitz SW, et al. Glioblastoma: a method for predicting response to antiangiogenic chemotherapy by using MR perfusion imaging--pilot study. Radiology 2010;255(2):622–628.

43. Hirai T, Murakami R, Nakamura H, et al. Prognostic value of perfusion MR imaging of high-grade astrocytomas: long-term follow-up study. AJNR Am J Neuroradiol 2008;29(8):1505–1510.

44. Jain R, Poisson L, Narang J, et al. Genomic mapping and survival prediction in glioblastoma: molecular subclassification strengthened by hemodynamic imaging biomarkers. Radiology 2013;267(1):212–220 .